Available online at www.sciencedirect.com
ScienceDirect
Trans. Nonferrous Met. Soc. China 32(2022) 2814−2827
Transactions of Nonferrous Metals Society of China
www.tnmsc.cn

Microstructure homogeneity regulation of 7050 aluminum forgings by surface cumulative plastic deformation

Jian-liang HU[1,2], Zi-han ZHAO[1], Meng-xiao DONG[1], Huan WANG[1], Miao JIN[1], Shi-quan HUANG[2], Hong BO[3]

1. School of Mechanical Engineering, Yanshan University, Qinhuangdao 066004, China;
2. State Key Laboratory of High Performance Complex Manufacturing, Central South University, Changsha 410083, China;
3. State Key Laboratory of Metastable Materials Science and Technology, Yanshan University, Qinhuangdao 066004, China

Received 23 August 2021; accepted 30 December 2021

Abstract: To regulate the microstructure homogeneity of large aluminum structural forgings for aircraft, the surface cumulative plastic deformation was proposed. The microstructure of 7050 aluminum forgings after the surface cumulative plastic deformation was investigated by electron backscatter diffraction (EBSD), transmission electron microscopy (TEM), and X-ray diffraction (XRD). The results showed that the microstructure evolution of 7050 aluminum forgings was more sensitive to the deformation temperature than the strain rate. The dislocation density continued to increase with the decrease of the deformation temperature and the increase of the strain rate. Dislocation density and stored energy were accumulated by the surface cumulative plastic deformation. Besides, a static recrystallization (SRX) model of 7050 aluminum forgings was established. The SRX volume fraction calculated by this model was in good agreement with the experimental results, which indicated that the model could accurately describe the SRX behavior of 7050 aluminum forgings during the surface cumulative plastic deformation.

Key words: microstructure homogeneity regulation; surface cumulative plastic deformation; dislocation density; static recrystallization model

1 Introduction

7050 aluminum alloy has been widely used in the aerospace field due to its high strength and toughness, excellent plasticity and heat-treatment [1,2]. At present, with the rapid development of the aviation industry, the 7050 aluminum alloy structural parts are forced to develop into the direction of large-scale integration, high precision and quality [3]. Therefore, a higher requirement is put forward for the macro- and micro-structural properties of aluminum structural parts [4,5].

However, the problem of coarse grains on the surface of forgings is quite common in the hot die forging process of aluminum structural parts [6]. Usually, coarse grains seriously weaken the service performance of aviation structural parts which need to be removed entirely by a subsequent mechanical process. Even serious defect causes forgings to be scrapped, resulting in a significant reduction in the utilization rate of aviation materials [7].

In recent years, research on the regulation of microstructure uniformity of forgings has been conducted [8]. There are mainly two common methods for practical grain refinement [9]. One is to achieve grain refinement through the dynamic recrystallization (DRX) caused by the large plastic deformation [10], the other is to improve the

Corresponding author: Hong BO, E-mail: bohong@ysu.edu.cn
DOI: 10.1016/S1003-6326(22)65985-5

uniformity of forgings through the isothermal die forging process [11]. The method of refining grains through large plastic deformation is widely used in actual production [12,13]. For example, SAKAI et al [14] used a multi-directional die forging process to perform high temperature large deformation of 7074 aluminum alloy with a total strain of 6.3. The results showed that under the condition of a lower strain rate, the alloy underwent continuous DRX, which realized grain refinement. SU et al [15] showed that the formation of refined grains was caused by constant DRX. With the strain accumulation, small-angle grain boundaries were gradually generated and continuously transformed into large-angle grain boundaries. The increase of large-angle grain boundaries led to a rise in the average orientation angle, thereby achieving grain refinement. Forgings were formed at a low strain under constant temperature conditions, avoiding the nonuniformity temperature caused by mold chilling and latent deformation heat. Therefore, the uniformity of the forging was improved. ZHAO et al [16] conducted isothermal precision forging of Al−Zn−Mg−Cu support bracket forging by finite element simulation and experiment. They found that more fine grains were formed in the forging that precision-forged at the transient speed as compared with that at the rate of 0.01 mm/s, which led to higher mechanical properties. HU et al [17] studied the evolution of the microstructure during the hot die forging process of 7A85 aluminum alloy. They found that during the hot deformation process of 7A85 aluminum alloy, dynamic recovery and dynamic recrystallization were the main mechanisms of microstructure evolution. ZHANG et al [18] studied the microstructural evolution and tensile properties of Ti−6Al−4V alloy during the multidirectional isothermal forging (MDIF). After three steps of isothermal forging, a homogeneous equiaxed grained microstructure with an average grain size of 1.9 mm was achieved.

Although the homogeneity regulation can be achieved through large plastic deformation or the isothermal die forging process, the two processes are complicated with long production cycles and low efficiency. Neither is suitable for the industrialized mass production of large aerospace die forgings.

Unlike the high temperature and large deformation, in this work, a new method named the surface cumulative plastic deformation was proposed to regulate the microstructure homogeneity for large aluminum forgings in aerospace after the traditional hot die forging process, which is shown schematically in Fig. 1. Unlike the traditional hot forging process, the surface cumulative plastic deformation is warm deformation of low height reduction. The dislocation density and stored energy are accumulated by surface cumulative plastic deformation. Therefore,

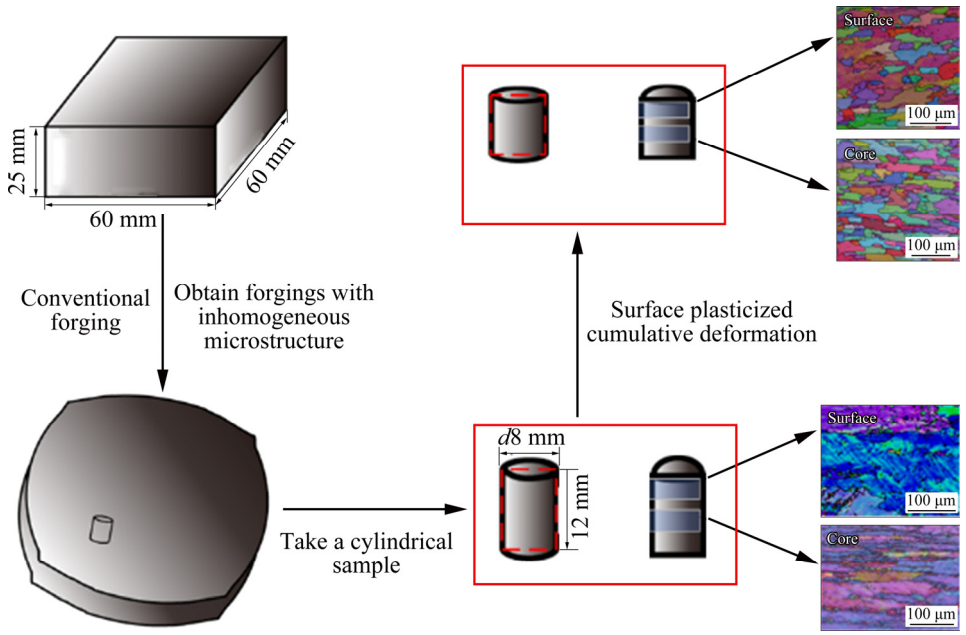

Fig. 1 Schematic diagram of surface plastic cumulative deformation process

static recrystallization is promoted to achieve the microstructure homogenization. We hope that the surface cumulative plastic deformation can regulate forgings with coarse surface microstructures. Many recrystallization models, including deformation parameters except dislocation density, have been established [19]. Based on the study of the grain evolution during the surface cumulative plastic deformation, an SRX model for 7050 aluminum alloy forgings, including dislocation density, was established.

2 Experimental

The chemical composition of annealed cuboid 7050 aluminum alloy billets employed in this study is listed in Table 1.

Table 1 Chemical composition of 7050 aluminum alloy billet (wt.%)

Zn	Mg	Cu	Si	Fe	Cr	Mn	Al
6.2	2.1	2.3	0.03	0.08	0.01	0.01	Bal.

Aluminum alloy billets were heated to 450 °C and kept for 2 h. Then, billets were subjected to a conventional hot die forging experiment with 50% height reduction on the die forging press to obtain forgings with inhomogeneous microstructure, as shown in Fig. 1. The billet was machined into cylindrical specimens of 8 mm in diameter and 12 mm in height along the forging direction. The surface cumulative plastic deformation of samples was conducted on the Gleeble−3800 simulation test machine with the height reductions of 10%, 20% and 30%, respectively, the deformation temperatures were 150, 200, 250, 300 and 350 °C, and the strain rates were 1, 0.1, 0.01 and 0.001 s^{-1}. Before the deformation, the polished ends of samples were attached with a graphite sheet and coated with high-temperature lubricant to ensure stability and uniformity. The samples were heated to the experimental temperature at a rate of 5 °C/s and held for 5 min to ensure uniform heating. All deformed samples were quenched immediately after deformation. Subsequently, the samples underwent the solution treatment and two-stage aging treatment, which were treated at 470 °C for 2 h in the solution treatment; the first aging treatment was 121 °C for 12 h, and the second aging process was 177 °C for 12 h.

The deformed samples for microstructural observation (EBSD and TEM) were sectioned perpendicularly to the compression axis from the core of the cylindrical specimen after the hot compression experiments. Half of them were treated with solution aging treatment, and the other part was untreated. The grain structures were characterized by electron backscattered diffraction (EBSD) in an OXFORD device equipped with an HKL Channel 5 EBSD System at an acceleration voltage of 20 kV. The EBSD samples were prepared by mechanical and electrochemical polishing. The TEM examinations were performed using the Tecnai-G220 microscope operated at 200 kV. For the XRD examinations, they were performed on the D/max2500 PC X-ray diffractometer with Cu target operated at 200 mA and 40 kV. The scanning wavelength (λ) is 1.5406 Å, the scanning range is 30°−90°, and the scanning adopts step-by-step scanning with a step length of 0.02°.

3 Results and discussion

3.1 Stress−strain curves of 7050 alloy during surface cumulative plastic deformation

Figure 2 shows the stress−strain curves obtained by the surface cumulative plastic deformation of 7050 aluminum forgings with 20% height reduction. With the increase of deformation temperature, the flow stress gradually decreases. The curve exhibits a continuous hardening trend during the deformation process at low temperatures (150 and 200 °C), especially at a higher strain rate, as seen from Fig. 2, which indicates that the dislocation density inside the alloy continues to accumulate during the deformation process. Subsequently, many dislocations produced by the deformation are entangled with each other, which inhibits the further migration of the dislocations. In addition, the tangle of dislocations results in the constant growth of flow stress. At the same time, the accumulation of a large number of dislocations also leads to the continuous increase of deformation energy storage. Forgings undergo complete SRX during the subsequent solution treatment process. At higher deformation temperatures (250, 300, and 350 °C), the curve shows apparent softening in the later deformation stage. On the other hand, forgings undergo a sufficient dynamic recovery at higher deformation temperatures, which entails the migration and offset of many dislocations. Therefore,

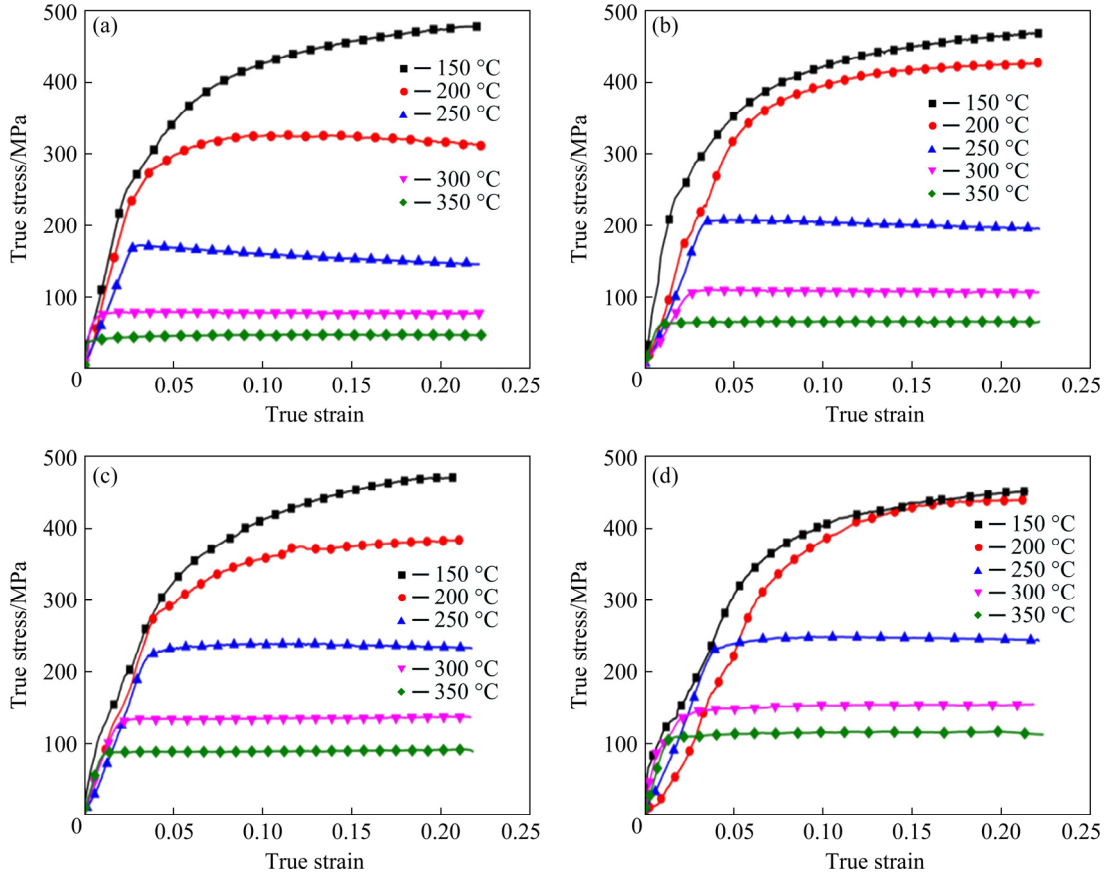

Fig. 2 True stress−true strain curves of 7050 aluminum alloy at temperatures from 150 to 350 °C under strain rates of 0.001 s^{-1} (a), 0.01 s^{-1} (b), 0.1 s^{-1} (c), and 1 s^{-1} (d)

amounts of dislocations are consumed, resulting in the continuous reduction of the deformation storage energy inside the alloy. As a result, the deformation storage energy is not enough to support the complete SRX of the alloy during the subsequent solution treatment process.

3.2 Microstructure evolution of 7050 alloy during surface cumulative plastic deformation

The DRX temperature of the seven series aluminum alloy is above 350 °C [20,21]. The maximum deformation temperature is only 350 °C, and the maximum height reduction is 30%. Under this condition, DRX does not tend to occur during the deformation. When the height reduction is 30% at 350 °C, the DRX volume fraction of the surface is 0.87%, and that of the core is 2.05%. Therefore, the DRX volume fraction is so small which can be ignored. Figure 3 shows the EBSD images of forgings at different deformation temperatures under the strain rate of 1 s^{-1}. The surface microstructure of the forging is consistent with the initial microstructure at the deformation temperature of 150 °C. When the deformation temperature rises to 200 °C, the surface grains are squashed, and the grain boundaries are broken. The deformation of surface grains increases wtih increasing the deformation temperature. On the contrary, the deformation pattern of the grains in the center of the forgings does not change with deformation temperature. As the deformation temperature increases, the dynamic recovery of the alloy increases, a large number of dislocations slip and climb, and grain boundary migration gets easier to proceed. In addition, the coarse and insoluble precipitated phases are unevenly distributed along the grain boundaries during the deformation process. Part of the grain boundaries is pinned, leading to a difficult migration of the grain boundaries. Therefore, the grain boundary changes in the width direction and appears to be jagged.

The EBSD images of heat-treated forgings after the surface cumulative plastic deformation with the strain rate of 1 s^{-1} are shown in Fig. 4. The EBSD maps are obtained by superimposing Euler

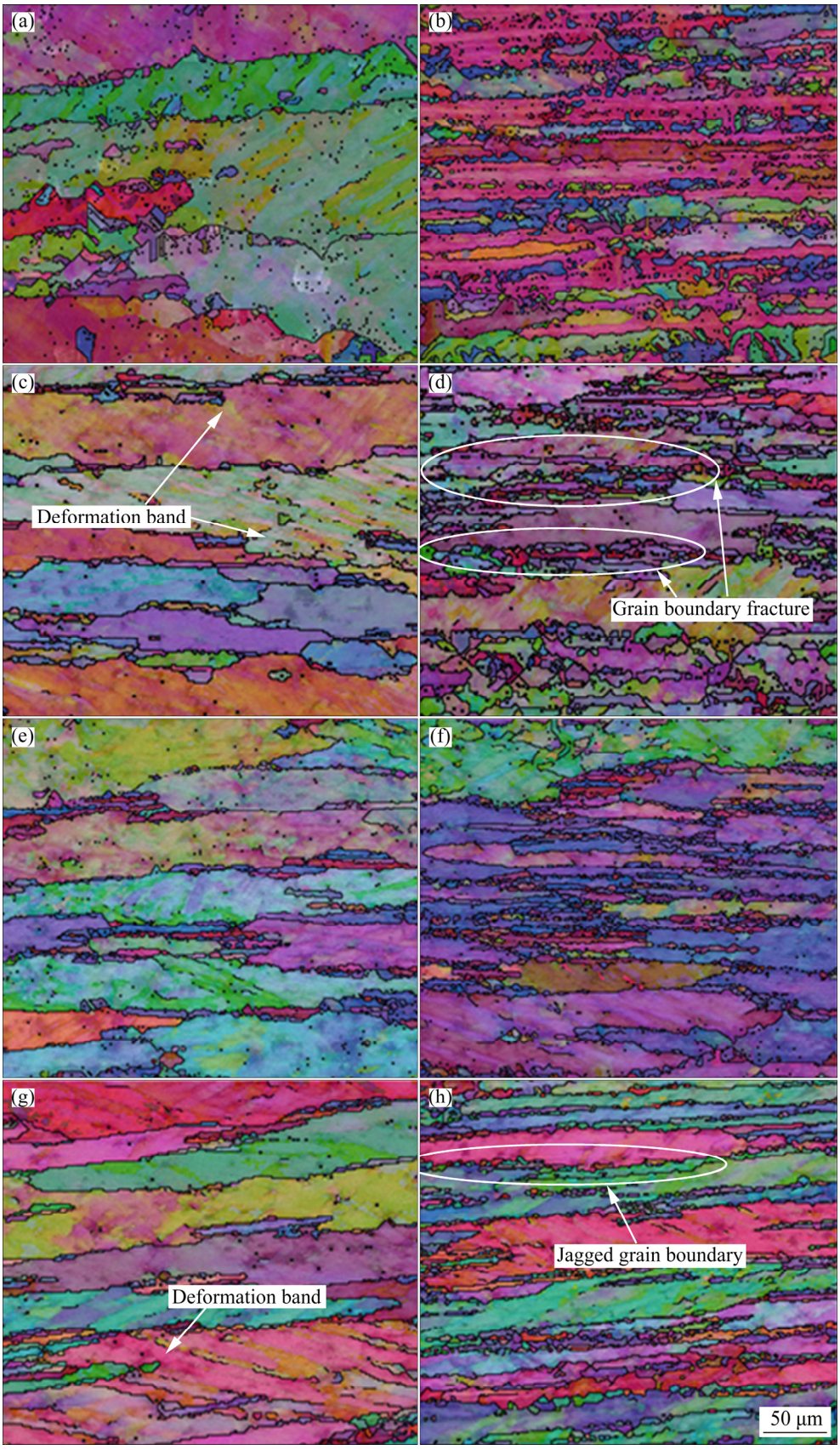

Fig. 3 EBSD images of forgings at different temperatures under strain rate of 1 s^{-1}: (a) Surface at 150 °C; (b) Core at 150 °C; (c) Surface at 200 °C; (d) Core at 200 °C; (e) Surface at 250 °C; (f) Core at 250 °C; (g) Surface at 300 °C; (h) Core at 300 °C

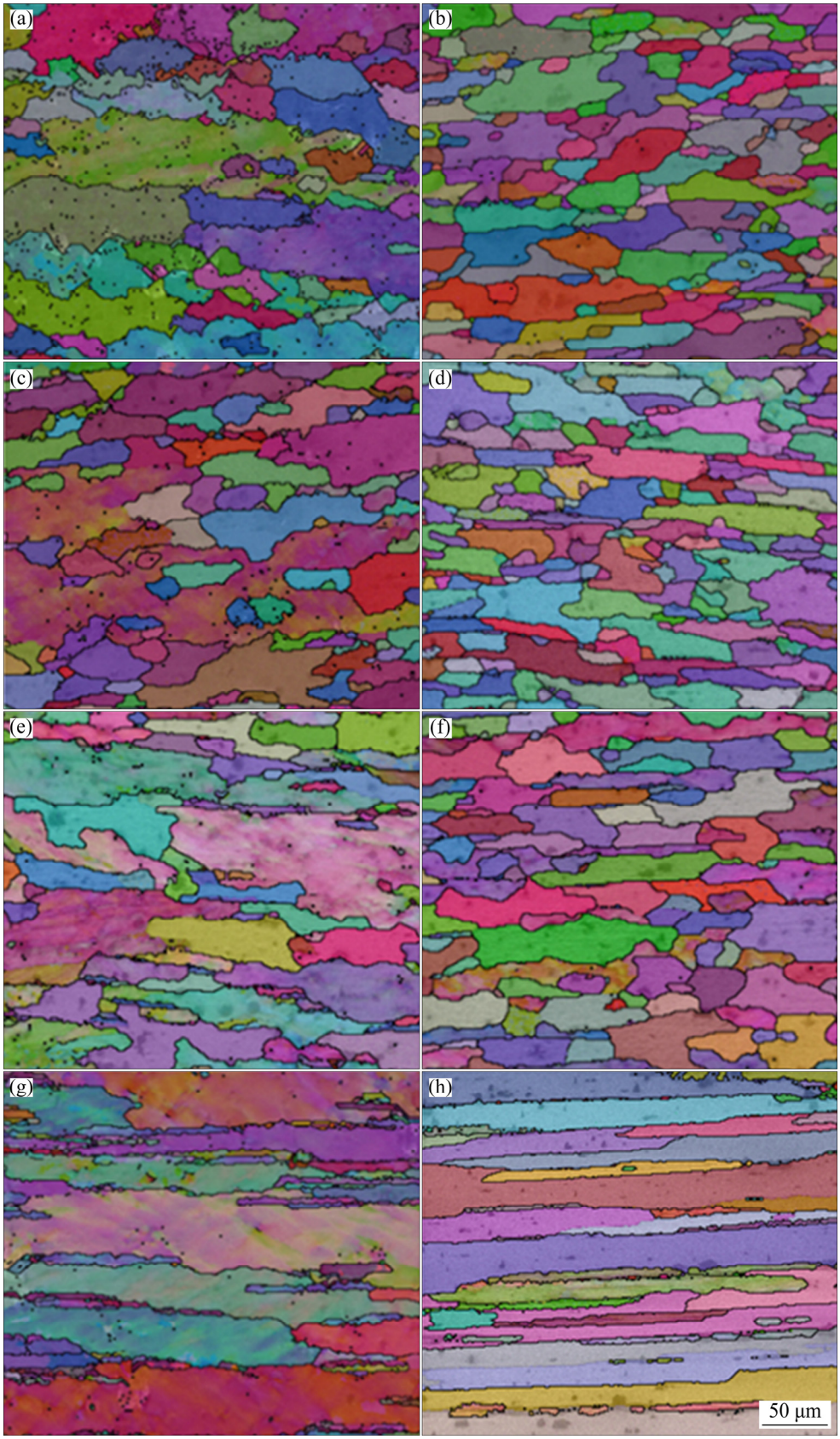

Fig. 4 EBSD images of solution-treated forgings at different temperatures under strain rate of 1 s^{-1}: (a) Surface at 150 °C; (b) Core at 150 °C; (c) Surface at 200 °C; (d) Core at 200 °C; (e) Surface at 250 °C; (f) Core at 250 °C; (g) Surface at 300 °C; (h) Core at 300 °C

angles and band contrast. In addition, the large-angle grain boundaries (>10°) are marked in the figures for microstructure analysis. The SRX degree in the lower deformation temperature is very high. There is a tendency for recrystallized grains to grow, as shown in Fig. 4(a). When the temperature rises to 200 and 250 °C, the growth of grains on the forging surface is inhibited. When the deformation temperature is 300 °C, the deformation storage energy is consumed during the deformation process. Grain growth occurs on the surface and core of the forging without SRX during the solution treatment process. When the deformation temperature is 200 °C, the grains of the forging tend to be uniform.

TEM images of 7050 aluminum forgings at different deformation temperatures are shown in Fig. 5. As the deformation temperature increases, the dislocation density and the corresponding dislocation entanglement gradually decrease. When the deformation temperature is 150 °C, many dislocations gather near the grain boundary and get entangled with each other. As the deformation temperature increases, grain boundary migration is easier to proceed. Consequently, many dislocations are offset. At the same time, many entangled dislocations slip and climb to form a dislocation wall and finally evolve into a dislocation cell. In

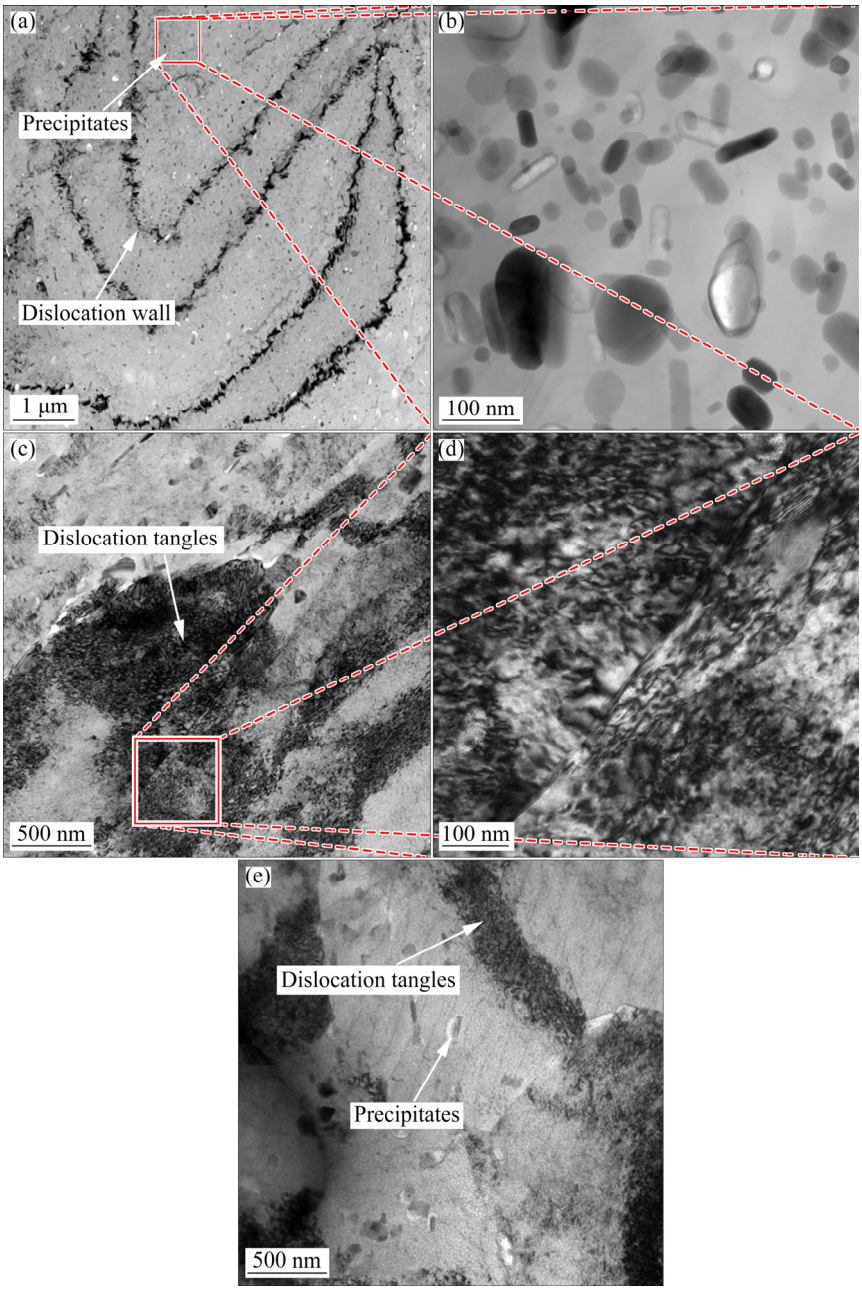

Fig. 5 TEM images of forgings under strain rate 1 s^{-1} at different temperatures: (a, b) 300 °C; (c, d) 200 °C; (e) 150 °C

addition, the size of the precipitated phase becomes larger. When the temperature rises to 200 °C, many dislocation walls and dislocation cells are formed. When the temperature reaches up to 300 °C, the dynamic recovery further enhances the merging and growth of dislocation cells. The merging of dislocation cells is caused by the migration of dislocation walls, which consumes a large amount of deformation and storage energy. Ultimately, the SRX of forgings during the solution treatment process is reduced.

According to the TEM images shown in Fig. 6, as the strain rate decreases, dislocation walls gradually form dislocation cells. This process is accompanied by the merging and growth of dislocation cells. At the strain rate of 0.1 s^{-1} or 0.01 s^{-1}, the main microstructure components are dislocation walls and a small number of delicate dislocation cells. And the large-scale dislocation entanglement disappears. As the strain rate decreases, the dynamic recovery of the forging intensifies, and the dislocations migrate and offset, leading to the decrease of the dislocation density. Meanwhile, the dislocation walls undergo significant migration and gradually transform into dislocation cells. When the strain rate is further reduced to 0.001 s^{-1}, the dynamic recovery is more violent. The migration of dislocations and dislocation walls is more likely to proceed, resulting in the merging of dislocation cells. Additionally, the size of dislocation cells increases significantly.

The dislocation density of 7050 aluminum alloy forgings after surface cumulative plastic deformation was calculated through the XRD experiments. As shown in Fig. 7, with the increase of the deformation temperature and the decrease of the strain rate, the dislocation density of the alloy shows a continuous decreasing trend. The dislocation density continues to decrease from 2.25×10^{14} to 1.57×10^{14} m^{-2} when the deformation temperature rises from 150 to 300 °C. The reduction of dislocation density means decreasing deformation storage energy during the deformation

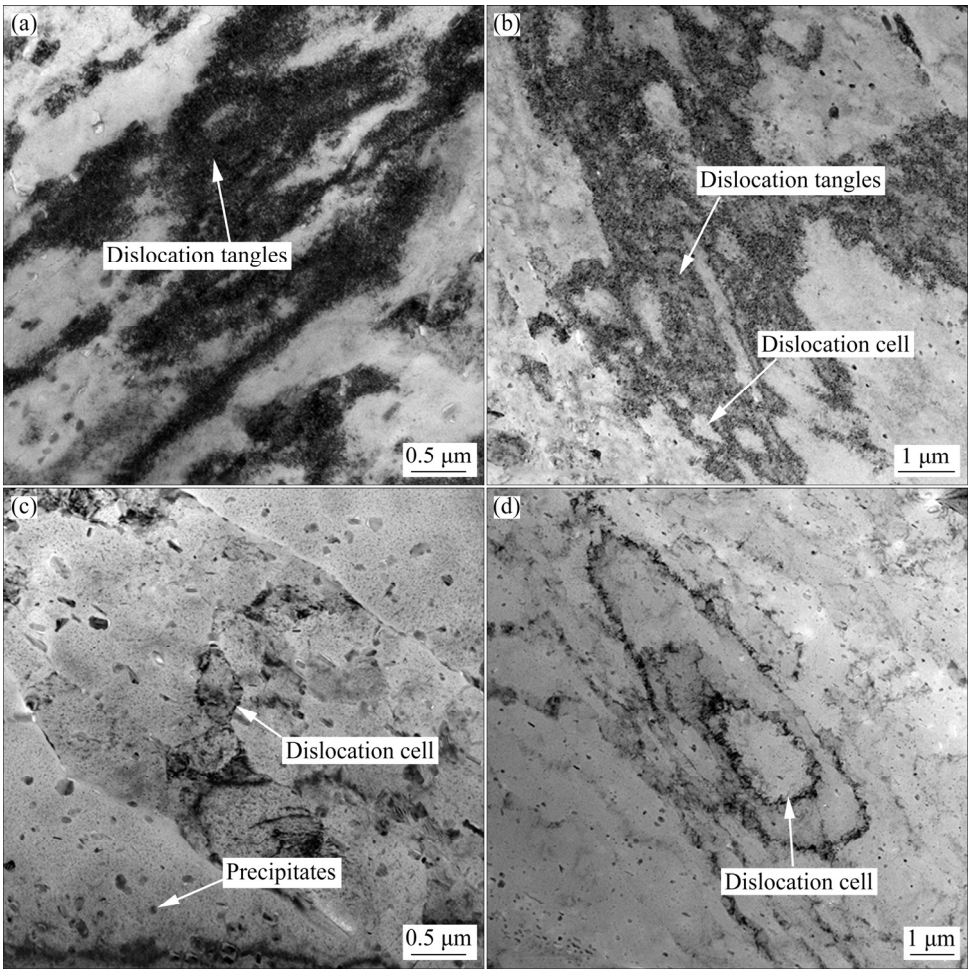

Fig. 6 TEM images of forgings at 220 °C under strain rate of 1 s^{-1} (a), 0.1 s^{-1} (b), 0.01 s^{-1} (c), and 0.001s^{-1} (d)

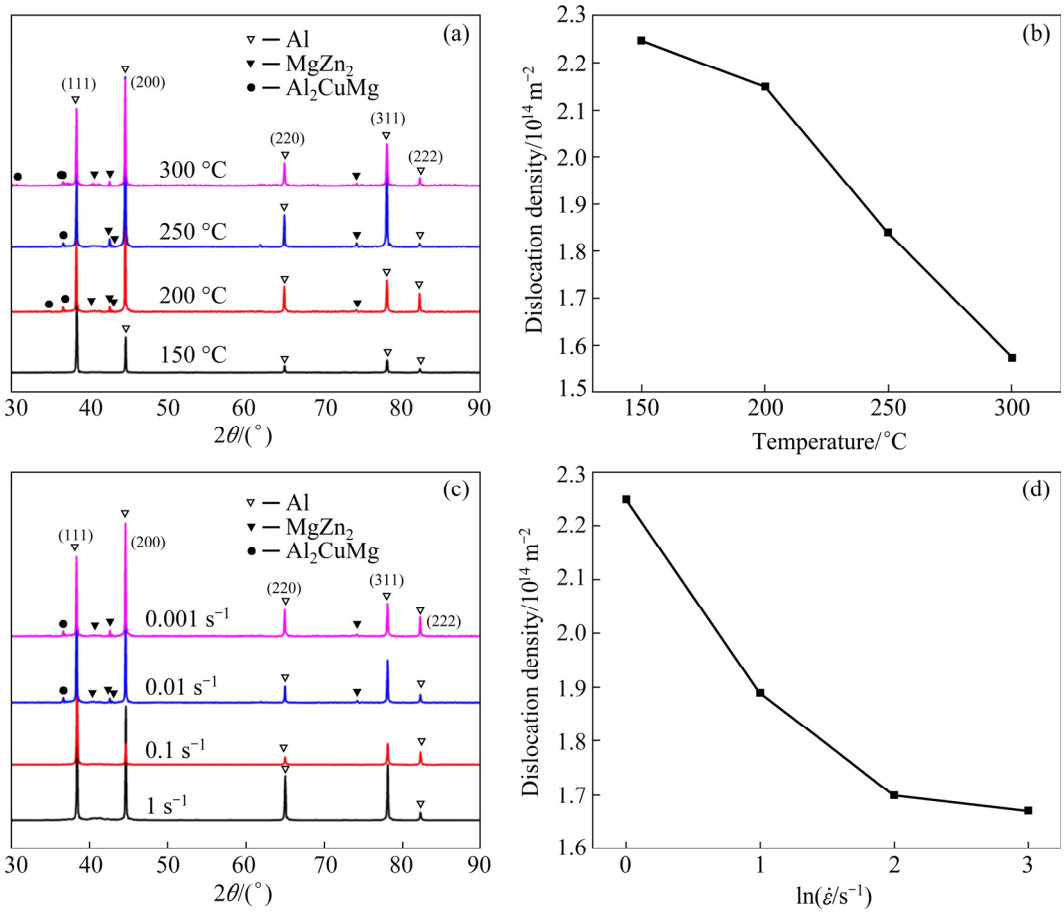

Fig. 7 XRD patterns (a, c) and dislocation density values (b, d) under different deformation conditions: (a, b) Deformation temperature; (c, d) Strain rate

process. As the strain rate decreases, the dislocation density of forgings continues to decrease from 2.25×10^{14} to 1.67×10^{14} m^{-2}. Subsequently, the curve tends to decrease gently. This phenomenon indicates that the microstructure evolution of 7050 aluminum forgings is less affected by the strain rate than the deformation temperature. The microstructure homogeneity can be efficiently regulated by cumulative deformation of 20% height reduction at 200 °C, the large strain rate of 1 s^{-1}, and the solution treatment cooperatively.

3.3 Establishment of SRX model

Most studies have shown that SRX equation can be expressed by the Avrami equation [22,23]:

$$X_v = 1-\exp[-0.693(\frac{t}{t_{0.5}})^k] \quad (1)$$

where X_v is the fractional softening attributable to SRX, k is a material constant, t is the occurring time of SRX, and $t_{0.5}$ is the time corresponding to the SRX fraction of 50%, which can be expressed by

$$t_{0.5} = A_1\varepsilon^a Z^{b_1}\exp(\frac{Q}{RT_1}) \quad (2)$$

$$Q=(Q_I+3Q_v)/4 \quad (3)$$

where Q is the SRX apparent activation energy. It is the clear activation energy of the overall transformation. Generally speaking, it is difficult to be related to the recrystallization mechanism and is often not constant. Q_I is the SRX nucleation activation energy, and Q_v is the SRX growth activation energy. In most cases, Q_I and Q_v are approximately equal, and both increase with the degree of deformation. The overall kinetics of recrystallization depends on the nucleation and growth rate of recrystallization, so all factors that affect the nucleation and growth will affect the overall dynamics [24−26]. R is the molar gas constant, T_1 is the solution temperature, A_1, a and b_1 are material-related constants, ε is the strain, and Z is the Zener–Hollomon parameter which can be expressed as

$$Z=\dot{\varepsilon}\exp(\frac{Q_1}{RT})=A_2\sigma^n \quad (4)$$

$$Z=\dot{\varepsilon}\exp(\frac{Q_1}{RT})=A_3\exp(\beta\sigma) \quad (5)$$

$$Z=\dot{\varepsilon}\exp(\frac{Q_1}{RT})=A_4[\sinh(\alpha\sigma)]^n \quad (6)$$

where A_2, A_3, A_4, β, α and n are material constants, $\dot{\varepsilon}$ is the strain rate, Q_1 is the deformation activation energy, T is the deformation temperature, and σ is the peak stress. To simplify the calculation, it is assume that,

$$\ln\dot{\varepsilon}=\ln B_1+n\ln\sigma \quad (7)$$

$$\ln\dot{\varepsilon}=\ln B_2+\beta\sigma \quad (8)$$

By processing the true stress−strain curves (Fig. 2), the relationship between the parameters in Fig. 8 is obtained. According to Fig. 8 and $\alpha=\beta/n$, it is calculated that β=0.0667, n=8.18, and α=0.008. Through the linear regression analysis of Fig. 9, Q_1=364 kJ/mol, A_4=2.96, and n=0.095 are obtained.

According to the classical Taylor relationship,

$$\sigma=M\alpha'\mu b\rho^{1/2} \quad (9)$$

where M is the Taylor factor, μ is the shear modulus, b is the magnitude of Persian vector, α' is the material constant, generally about 0.5, and ρ is the dislocation density. Therefore, the Z parameter can be expressed by the relational expression, including the dislocation density:

$$Z=2.96[\sinh(0.004Mb\rho^{1/2})]^{0.095} \quad (10)$$

The aluminum forgings deformed under different deformation conditions were subjected to solution treatment at different temperatures for different time. The SRX degree was counted, and the time to reach 50% under each condition was obtained. The results are shown in Fig. 10.

According to the above results, the SRX model of 7050 aluminum alloy can be expressed as [27]

$$X_v=1-\exp[-0.693(\frac{t}{t_{0.5}})^{0.544}] \quad (11)$$

$$t_{0.5}=6.37\times10^{-9}\varepsilon^{-0.47}\cdot[\sinh(0.004M\mu b\rho^{1/2})^{-0.00228}]\exp(\frac{127000}{RT}) \quad (12)$$

3.4 Model verification and discussion

The SRX volume fractions under different deformation temperatures, height reductions, strain rates and heat treatment temperature conditions are calculated by the SRX model, as shown in Fig. 11.

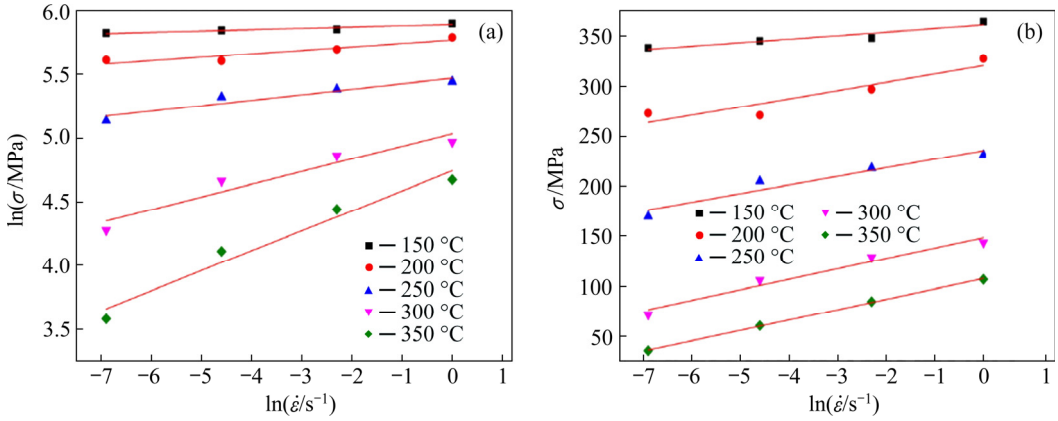

Fig. 8 Relationship of $\ln\sigma$ and $\ln\dot{\varepsilon}$ (a), and σ and $\ln\dot{\varepsilon}$ (b)

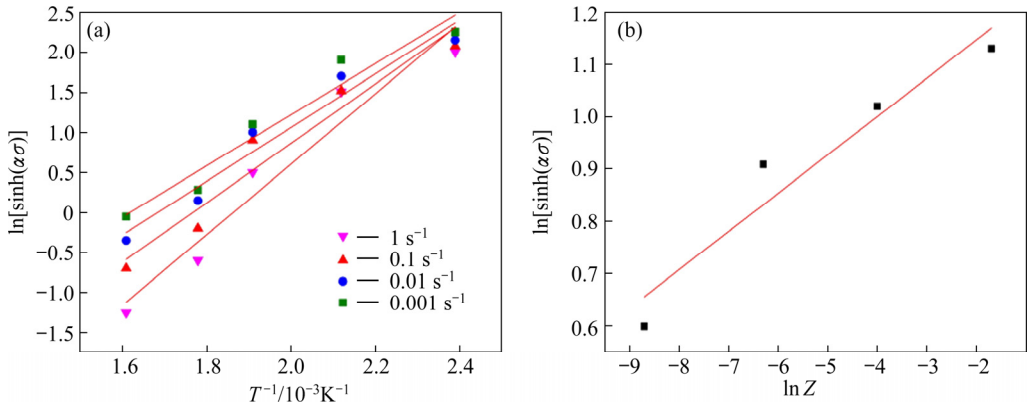

Fig. 9 Relationship of $\ln[\sinh(\alpha\sigma)]-1/T$ (a), and $\ln[\sinh(\alpha\sigma)]-\ln Z$ (b)

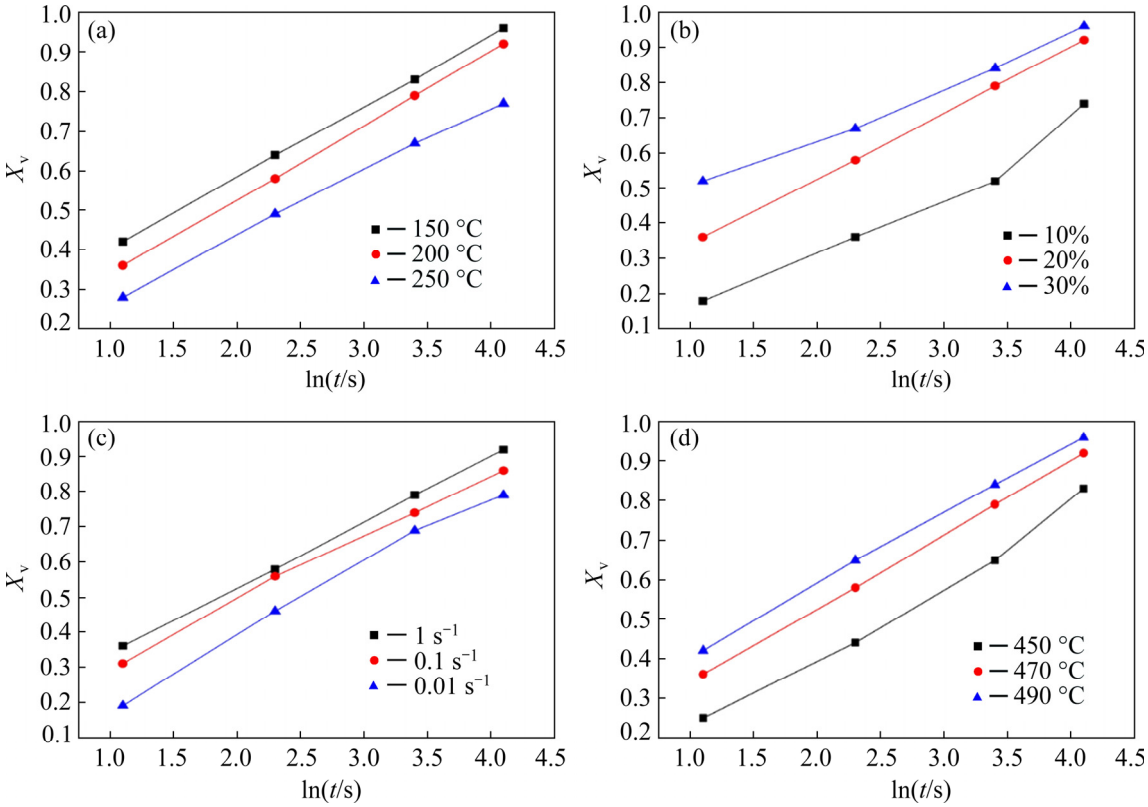

Fig. 10 Degree of SRX affected by deformation temperature (a), height reduction (b), strain rate (c), and solution temperature (d)

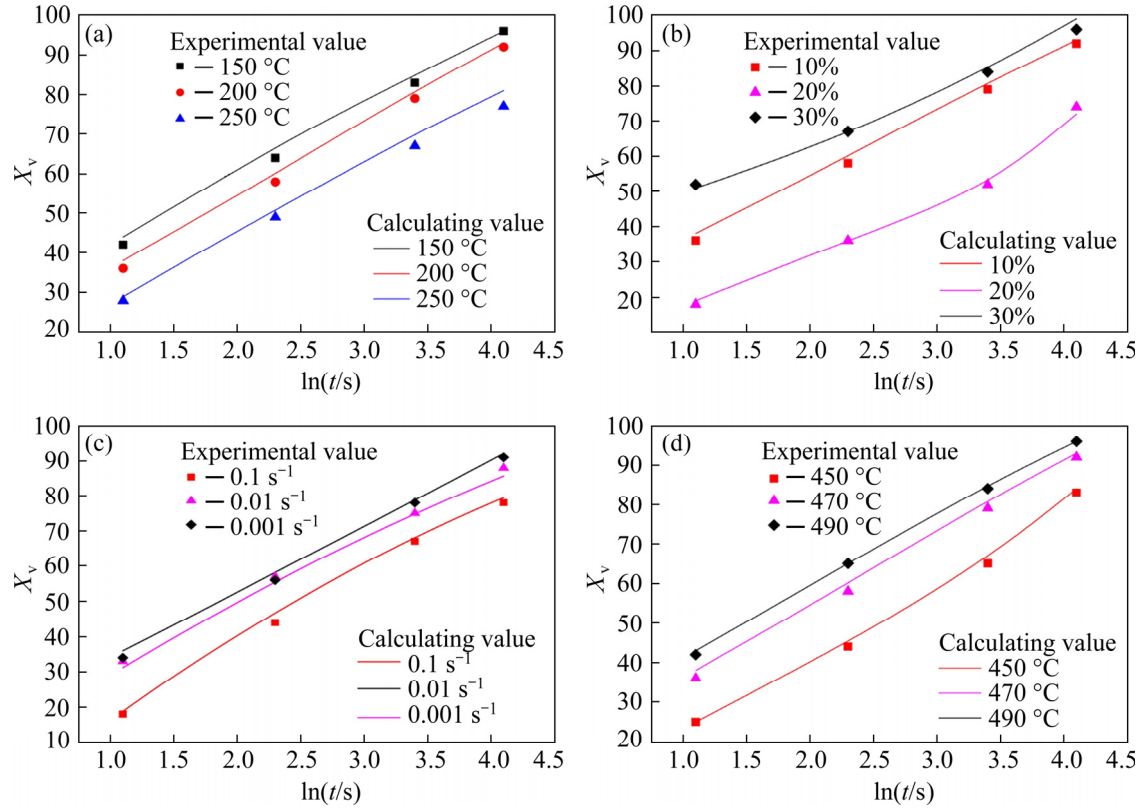

Fig. 11 Comparison between calculated and experimental values of static recrystallization volume fraction under different deformation temperatures (a), height reductions (b), strain rates (c), and solution temperatures (d)

It can be seen that the computed SRX volume fractions under various deformation conditions are in good agreement with the experimental values, indicating that the established SRX model can accurately predict the SRX degree of 7050 aluminum forgings after the surface cumulative plastic deformation (Tables 2−5).

Table 2 Prediction error of SRX volume fraction at different deformation temperatures

Deformation temperature/°C	Mean absolute error/%
150	0.091
200	0.011
250	0.499

Table 3 Prediction error of SRX volume fraction at different height reductions

Height reduction/%	Mean absolute error/%
10	0.011
20	0.235
30	1.026

Table 4 Prediction error of SRX volume fraction at different strain rates

Strain rate/s^{-1}	Mean absolute error/%
0.1	0.005
0.01	0.383
0.001	0.0023

Table 5 Prediction error of SRX volume fraction at different solution temperatures

Solution temperature/°C	Mean absolute error/%
450	0.018
470	0.011
490	0.025

4 Conclusions

(1) The microstructure evolution of 7050 aluminum forgings is more sensitive to the deformation temperature than the strain rate. The dislocation density continues to increase with the decrease of the deformation temperature and the increase of the strain rate. The dislocation density and stored energy accumulated during the surface cumulative plastic deformation. Therefore, the SRX is promoted to achieve the microstructure homogenization.

(2) The influence of the surface cumulative plastic deformation on the grain evolution of 7050 aluminum forgings has been studied. The SRX model of 7050 aluminum forgings with dislocation density is established.

(3) The model has been used to calculate the SRX volume fraction of the surface layer of aluminum alloy samples at different deformation temperatures, height reductions, strain rates and solution treatment temperatures. The results show that the calculated values are in good agreement with the experimental values, indicating that the established SRX model can accurately describe the SRX behavior of the 7050 aluminum forging.

Acknowledgments

This work was supported by the Natural Science Foundation of Hebei Province, China (No. E2019203075), the Top Young Talents Project of the Education Department of Hebei Province, China (No. BJ2019001), and the State Key Laboratory Program of High Performance Complex Manufacturing, China (No. Kfkt2017-07).

References

[1] DURSUN T, SOUTIS C. Recent developments in advanced aircraft aluminium alloys [J]. Materials & Design, 2014, 56: 862−869. https://doi.org/10.1016/j.matdes.2013.12.002.

[2] NEWMAN J C Jr, ANAGNOSTOU E L, RUSK D. Fatigue and crack-growth analyses on 7075-T651 aluminum alloy coupons under constant- and variable-amplitude loading [J]. International Journal of Fatigue, 2014, 62: 133−143. https://doi.org/10.1016/j.ijfatigue.2013.04.020.

[3] LI C B, WANG S L, ZHANG D Z, LIU S D, SHAN Z J, ZHANG X M. Effect of Zener−Hollomon parameter on quench sensitivity of 7085 aluminum alloy [J]. Journal of Alloys and Compounds, 2016, 688: 456−462. https://doi.org/10.1016/j.jallcom.2016.07.089.

[4] ZHANG Y, MILKEREIT B, KESSLER O, SCHICK C, ROMETSCH P A. Development of continuous cooling precipitation diagrams for aluminium alloys AA7150 and AA7020 [J]. Journal of Alloys and Compounds, 2014, 584: 581−589. https://doi.org/10.1016/j.jallcom.2013.09.014.

[5] ESTRIN Y, VINOGRADOV A. Extreme grain refinement by severe plastic deformation a wealth of challenging science [J]. Acta Materialia, 2013, 61(3): 782−817. https://doi.org/10.1016/j.actamat.2012.10.038.

[6] PANIGRAHI S K, JAYAGANTHAN R. Development of ultrafine-grained Al6063 alloy by cryorolling with the optimized initial heat treatment conditions [J]. Materials &

Design, 2011, 32(4): 2172−2180. https://doi.org/10.1016/j.matdes.2010.11.027.

[7] XU R, LIN B, LI H Y, XIAO H Q, ZHAO Y L, ZHANG W W. Microstructure evolution and mechanical properties of Al−6.5Cu−0.6Mn−0.5Fe alloys with different Si additions [J]. Transactions of Nonferrous Metals Society of China, 2019, 29(8): 1583−1591. https://doi.org/10.1016/S1003-6326(19)65065-X.

[8] SHE X W, JIANG X Q, WANG P Q, TANG B B, CHEN K, LIU Y J, CAO W N. Relationship between microstructure and mechanical properties of 5083 aluminum alloy thick plate [J]. Transactions of Nonferrous Metals Society of China, 2020, 30(7): 1780−1789. https://doi.org/10.1016/S1003-6326(20)65338-9.

[9] BELYAKOV A, KIMURA Y, TSUZAKI K. Recovery and recrystallization in ferritic stainless steel after large strain deformation [J]. Materials Science and Engineering A, 2005, 403(1/2): 249−259. https://doi.org/10.1016/j.msea.2005.05.057.

[10] GUO F, ZHANG D F, YANG X S, JIANG L Y, PAN F S. Strain-induced dynamic precipitation of Mg17Al12 phases in Mg–8Al alloys sheets rolled at 748 K [J]. Materials Science and Engineering A, 2015, 636(11): 516−521. https://doi.org/10.1016/j.msea.2015.03.112.

[11] SHI Z F, GUO H Z, LIU R, WANG X C, YAO Z K. Microstructure and mechanical properties of TC21 titanium alloy by near-isothermal forging [J]. Transactions of Nonferrous Metals Society of China, 2015, 25(1): 72−79. https://doi.org/10.1016/S1003-6326(15)63580-4.

[12] SHAN D B, XU W C, HAN X Z, HUANG X L. Study on isothermal precision forging process of rare earth intensifying magnesium alloy [J]. Materials Science and Engineering B, 2012, 177: 1698−1702. https://doi.org/10.1016/j.mseb.2011.10.006.

[13] MENG Y, SUGIYAMA S, TAN J B, YANAGIMOTO J. Effects of forming conditions on homogeneity of microstructure and mechanical properties of A6061 aluminum alloy manufactured by time-dependent rheoforging on a mechanical servo press [J]. Journal of Materials Processing Technology, 2014, 214: 3037−3047. https://doi.org/10.1016/j.jmatprotec.2014.07.014.

[14] SAKAI T, MIURA H, GOLOBORODKO A, SITDIKOV O. Continuous dynamic recrystallization during the transient severe deformation of aluminum alloy 7475 [J]. Acta Materialia, 2009, 57(1): 153−162. https://doi.org/10.1016/j.actamat.2008.09.001.

[15] SU N, GUAN R G, WANG X, WANG Y X, JIANG W S, LIU H N. Grain refinement in an AlEr alloy during accumulative continuous extrusion forming [J]. Journal of Alloys and Compounds, 2016, 680: 283−290. https://doi.org/10. 1016/j.jallcom.2016.04.137.

[16] ZHAO J H, DENG Y L, ZHANG J, TANG J G. Effect of forging speed on the formability, microstructure and mechanical properties of isothermal precision forged of Al−Zn−Mg−Cu alloy [J]. Materials Science and Engineering A, 2019, 767. https://doi.org/10.1016/j.msea.2019.138366.

[17] HU J L, WU X J, BO H, JIAO Z T, HUANG S Q, JIN M. Dislocation density model and microstructure of 7A85 aluminum alloy during thermal deformation [J]. Journal of Central South University, 2021, 28(10): 2999−3007. https://doi.org/10.1007/s11771-021-4832-5.

[18] ZHANG Z X, QU S J, FENG A H, HU X, SHEN J. Microstructural mechanisms during multidirectional isothermal forging of as-cast Ti−6Al−4V alloy with an initial lamellar microstructure [J]. Journal of Alloys and Compounds, 2019, 773: 277−287. https://doi.org/10.1016/j.jallcom. 2018.09.220.

[19] ZHANG Zhi-hao, HOU Wen-rong, PANG Qing-hai, XIE Jian-xin. The dynamic recrystallization model of 7050 Al-alloy during hot deformation [J]. Materials Science Forum, 2013, 749: 274−281. https://doi.org/10.4028/ www.scientific.net/MSF.749.274.

[20] LI J P, SHEN J, YAN X D, MAO B P, YAN L M. Microstructure evolution of 7050 aluminum alloy during hot deformation [J]. Transactions of Nonferrous Metals Society of China, 2010, 20(2): 189−194. https://doi.org/10.1016/S1003-6326(09)60119-9.

[21] YI You-ping, SHI Yan. Physical simulation of dynamic recrystallization behavior of 7050 aluminum alloy [J]. Materials Science Forum, 2008, 575/576/577/578: 1083−1085. https://doi.org/10.4028/www.scientific.net/MSF.575-578.1083.

[22] LI H P, GAI K, HE L F, ZHANG C Z, CUI H Z, LI M S. Non-isothermal phase-transformation kinetics model for evaluating the austenization of 55CrMo steel based on Johnson−Mehl−Avrami equation [J]. Materials & Design, 2016, 92: 731−741. https://doi.org/10.1016/j.matdes.2015.12.110.

[23] CHO S H, KANG K B, JONAS J J. Effect of manganese on recrystallisation kinetics of niobium microalloyed steel [J]. Materials Science and Technology, 2002, 18(4): 389−395. https://doi.org/10.1179/026708302225001859.

[24] WANG W X, ZHANG J X, WANG Z J, LIU W C. A comparative study of the transformation kinetics of recrystallization texture of CC and DC 3003 aluminum alloys [J]. Materials Characterization, 2018, 141: 412−422. https://doi.org/10.1016/j.matchar.2018.05.011.

[25] SHEN W F, ZHANG C, ZHANG L W, XU Q H, CUI Y, XU Y F. A modified Avrami equation for kinetics of static recrystallization of Nb−V microalloyed steel: Experiments and numerical simulation [J]. Vacuum, 2018, 150: 116−123. https://doi.org/10.1016/j.vacuum.2018.01.022.

[26] LANG E, CANETOLI S. Microcalorimetric investigation of the recrystallization behaviour of polycrystalline copper deformed at room-temperature [J]. Journal of Thermal Analysis, 1976, 10(1): 27−36. https://doi.org/10.1007/BF02179187.

[27] ZHAO M J, HUANG L, ZENG R, WEN D X, SU H L, LI J J. In-situ observations and modeling of static recrystallization in 300 M steel [J]. Materials Science and Engineering A, 2019, 765: 138300. https://doi.org/10.1016/j.msea. 2019.138300.

7050 铝合金锻件显微组织均匀性的表层增塑累积变形调控

胡建良[1,2]，赵子寒[1]，董梦晓[1]，王 欢[1]，金 淼[1]，黄始全[2]，薄 宏[3]

1. 燕山大学 机械工程学院，秦皇岛 066004；
2. 中南大学 高性能复杂制造国家重点实验室，长沙 410083；
3. 燕山大学 亚稳态材料科学与技术国家重点实验室，秦皇岛 066004

摘 要：为调控大型飞机用铝合金结构件的组织均匀性，提出表层增塑累积变形的方法。采用电子背散射衍射、透射电子显微镜和 X 射线衍射技术研究 7050 铝合金锻件表层增塑累积变形后的显微组织。结果表明，7050 铝合金锻件的显微组织演变对变形温度比应变速率更敏感。锻件的位错密度随着变形温度的降低和应变速率的增加而持续增加。通过表层增塑累积变形实现位错密度和形变储能的高效累积。此外，建立 7050 铝合金的静态再结晶模型，计算得到的静态再结晶体积分数与实验结果吻合较好，说明该模型能够准确地描述 7050 铝合金在表层增塑累积变形调控中的静态再结晶行为。

关键词：显微组织均匀性调控；表层累积塑性变形；位错密度；静态再结晶模型

(Edited by Xiang-qun LI)